Inorganic Chemistry

pubs.acs.org/IC Article

Polymorphism and Molten Nitrate Salt-Assisted Single Crystal to Single Crystal Ion Exchange in the Cesium Ferrogermanate Zeotype: $CsFeGeO_4$

Mohammad Usman, Vancho Kocevski, Mark D. Smith, Gregory Morrison, Weiguo Zhang, Theodore Besmann, P. Shiv. Halasyamani, and Hans-Conrad zur Loye*

Cite This: *Inorg. Chem.* 2020, 59, 9699–9709 Read Online

ABSTRACT: Two polymorphs of a new cesium ferrogermanate zeotype, $CsFeGeO_4$, were synthesized using the molten CsCl-CsF flux growth approach at 900 °C. The orthorhombic polymorph, referred to as (**1**), crystallizes in the centrosymmetric nonpolar *Pbcm* space group. The compound exhibits a three-dimensional porous framework structure composed of disordered $(Fe/Ge)O_4$ corner-sharing tetrahedra that generate large eight-sided channels running down the *b*-axis. These channels are occupied by Cs ions that provide charge balance to the anionic framework. Minor modifications in the reaction conditions lead to the synthesis of a monoclinic polymorph of $CsFeGeO_4$, referred to as (**2**), crystallizing in the noncentrosymmetric polar space group $P2_1$ and exhibiting an identical framework structure to (**1**), albeit featuring ordered FeO_4 and GeO_4 tetrahedra. Solid state synthesis of $CsFeGeO_4$ produces a polycrystalline mixture of (**1**) and (**2**), referred to as (**6**). Polarization-electric field (P-E) measurements of (**6**) indicate that the material is not ferroelectric. Powder second harmonic generation (SHG) measurements of (**2**) and (**6**) revealed them to be SHG active with intensities of 1.5 and 0.2 times that of α-SiO_2, respectively. The temperature dependent magnetic susceptibility of (**2**) exhibits a downturn at T = 2.6 K, indicative of antiferromagnetic ordering. First-principles calculations in the form of density functional theory showed that (**1**) and (**2**) differ in stability by only 1.3 meV/atom, with (**2**) being the thermodynamically stabilized phase. Additional calculations for (**1**), using molten nitrate as reference, predicted the formation of energetically favorable phases, $KFeGeO_4$ (**3**) and $RbFeGeO_4$ (**4**). They were subsequently prepared via a molten nitrate salt bath treatment of (**1**) to replace Cs with K and Rb, affording (**3**) and (**4**) as single-crystal to single-crystal ion exchange products. Structure determination and property measurements for a pyroxene phase, $CsFeGe_2O_6$, referred to as (**5**), are also reported. This compound crystallized as a side product in the flux synthesis of $CsFeGeO_4$.

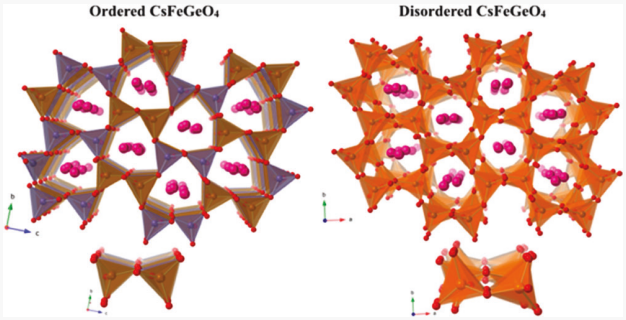

INTRODUCTION

Zeolites are a naturally occurring class of microporous, crystalline aluminosilicates that are produced commercially for their use in catalysis, gas adsorption, and ion-exchange applications.[1−3] Modifying aluminosilicates by introducing transition elements has always been of interest; however, attempts to incorporate, for example, iron into the aluminosilicate framework via hydrothermal routes have been met with limited success.[4−6] Nonetheless, the growth of single crystals of the first sodalite-type zeolite containing an all-iron framework, a ferrolite, $Ba_8(Fe_{12}O_{24})Na_y(OH)_6{\cdot}xH_2O$, was recently reported using a modified hydrothermal method, the hydroflux method, in nearly quantitative yield.[7] Achieving tetrahedral Fe(III) coordination in a normal hydrothermal environment appears difficult and is likely the chief impediment to the formation of iron-based zeolite-type, three-dimensional porous frameworks.

A large number of octahedrally coordinated iron containing silicates and germanates, on the other hand, are known and belong to an important group of minerals, the pyroxenes, with the general formula ABT_2O_6 (A = Na, Li, Ca, Sr; B = divalent and trivalent cations including Mg, Ni, Co, Fe, Mn, Al, Ga, Sc, In; and T = Si, Ge), which have been studied extensively in the geosciences for decades.[8] Compared to octahedrally coordinated iron-based silicates and germanates, there are very few tetrahedrally coordinated iron-based silicates and germanates known, either as polycrystalline powders or as single crystals.

Received: March 29, 2020
Published: July 2, 2020

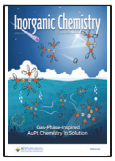

https://dx.doi.org/10.1021/acs.inorgchem.0c00936
Inorg. Chem. 2020, 59, 9699−9709

Scheme 1. Illustration of the Synthetic Routes for All Title Compounds

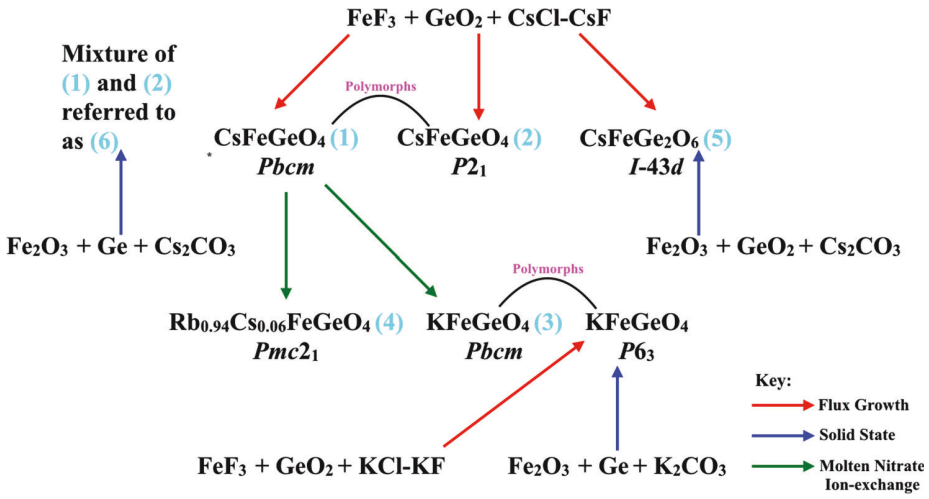

Table 1. Reagents and Reaction Conditions for (1)−(4)

compound	composition	reagents	flux[a]	temperature profile
(1)	orthorhombic $CsFeGeO_4$	1 mmol FeF_3 or 0.5 mmol Fe_2O_3	3.1 g CsCl-CsF eutectic	heated at 600 °C/h to 900 °C, held for 24 h and slow cooled to 400 °C at 6 °C/h
		1 mmol GeO_2		
(2)	monoclinic $CsFeGeO_4$	1 mmol FeF_3 or 0.5 mmol Fe_2O_3	1.8 g CsCl-CsF eutectic	heated at 600 °C/h to 900 °C, held for 12 h and slow cooled to 400 °C at 6 °C/h
		1 mmol GeO_2		
(3)	$KFeGeO_4$	0.1 g of compound (1)	1 g KNO_3	heated at 600 °C/h to 375 °C, held for 16 h and shut off
(4)	$Rb_{0.94}Cs_{0.06}FeGeO_4$	0.1 g of compound (1)	1 g $RbNO_3$	heated at 600 °C/h to 350 °C, held for 16 h and shut off

[a]Eutectic CsCl-CsF is 45% by mol of CsF with melting point = 486 °C.

Faust, in 1936, examined the equilibrium compositions of the ternary Fe_2O_3−K_2O−SiO_2 system and indicated the existence of $KFeSi_2O_6$ and iron feldspar $KFeSi_3O_8$.[9] More recently, Bentzen reported on three crystalline polymorphs of $KFeSiO_4$, a high temperature orthorhombic α-phase of unknown structure, a β-phase that adopts the tridymite structure, and a γ-phase that adopts the kaliophilite structure.[10] Clearly, it is possible, but apparently not easy, to synthesize new tetrahedrally coordinated iron based silicates and germanates aside from the well-known pyroxenes. Reports on new tetrahedrally coordinated iron silicates and germanates appeared as new synthetic routes were explored. $CsFeSiO_4$, a maximum iron content zeotype and structurally related to monoclinic $CsFeGeO_4$, presented herein, was prepared using a gel decomposition method followed by high temperature annealing, and its structure determined using Rietveld refinement of the polycrystalline product.[11] This work was soon followed up, and reports of hexagonal $KFeGeO_4$[12] and a feldspar, $KFeGe_3O_8$, appeared in the literature.[13]

We have been exploring the flux crystal growth of complex iron oxides, which resulted in numerous complex di, tri, and tetravalent iron oxides to date.[14−17] We continue to be interested in applying molten salt crystal growth approaches for the crystallization of new complex iron oxides and herein describe the use of alkali halide melts for their enhanced ability to solubilize halide or oxide precursors at relatively lower temperatures. Herein, we report on the flux growth synthesis and structural characterization of both $CsFeGeO_4$ polymorphs (**1**, **2**) and $CsFeGe_2O_6$ (**5**), a pyroxene, that crystallized as a minor phase during the $CsFeGeO_4$ flux synthesis reactions. We also highlight the conventional solid state synthesis for $CsFeGeO_4$ (**6**) which forms as a mixture of (**1**) and (**2**) due to their miniscule energy difference as determined by first-principles density functional theory (DFT) calculations carried out to calculate their thermodynamic stability. DFT calculations predicted the formation of $AFeGeO_4$ (A = K, Rb) from $CsFeGeO_4$ (**1**) via a molten nitrate salt ion exchange process. This process is not destructive, and it can be used for the single-crystal to single-crystal conversion of $CsFeGeO_4$ (**1**) into orthorhombic $KFeGeO_4$ (**3**), a kinetically stabilized polymorph of hexagonal $KFeGeO_4$,[12] as well as into orthorhombic $Rb_{0.94}Cs_{0.06}FeGeO_4$ (**4**). An overall illustration of the compounds, reported herein, and their syntheses and interconversions via molten nitrate salt ion exchange is provided in Scheme 1.

EXPERIMENTAL SECTION

Reagents. FeF_3 (99%, Strem), Fe_2O_3 (99.5%, Alfa Aesar), GeO_2 (99.999%, Alfa Aesar), Ge powder (99.999%, Cerac), KNO_3 (99.995%, Alfa Aesar), $RbNO_3$ (99%, Alfa Aesar), CsCl (Ultrapure, VWR), CsF (99.9%, Alfa Aesar), and Cs_2CO_3 (99.9%, Alfa Aesar) were used as received for all flux growth and solid state synthesis experiments.

Flux Growth Synthesis and Ion-Exchange. $CsFeGeO_4$ was prepared by a molten eutectic CsCl-CsF flux growth approach. (**1**) and (**2**) were synthesized by charging a 7.5 cm tall by 1.2 cm diameter cylindrical silver crucible with FeF_3 or Fe_2O_3 as the iron precursor, GeO_2, and the appropriate amount of CsCl-CsF flux. The silver crucible was placed into a programmable furnace and heated to the reaction temperature of 900 °C and held at this temperature for 24 h (**1**) and 12 h (**2**). Subsequently the reactions were slow cooled at 6°/h to 400 °C, whereupon the furnace was shut off.

https://dx.doi.org/10.1021/acs.inorgchem.0c00936
Inorg. Chem. 2020, 59, 9699−9709

Table 2. Crystallographic and Refinement Data for (1)−(5)

compound	(1)	(2)	(3)	(4)	(5)
composition	$CsFeGeO_4$	$CsFeGeO_4$	$KFeGeO_4$	$Rb_{0.94}Cs_{0.06}FeGeO_4$	$CsFeGe_2O_6$
T (K)			301 (2)		
crystal setting	Orthorhombic	Monoclinic	Orthorhombic	Orthorhombic	Cubic
space group	*Pbcm*	$P2_1$[a]	*Pbcm*	$Pmc2_1$[b]	*I*-43*d*
formula weight	325.35	325.35	231.54	280.86	429.94
crystal color and habit	yellow rod	gold brown block	brown rod	orange rod	gold polyhedron
a (Å)	9.5617(9)	9.2751(5)	9.1388(9)	8.9561(8)	14.0839(8)
b (Å)	5.6785(6)	5.6825(3)	5.5945(6)	9.3126(8)	14.0839(8)
c (Å)	18.5636(19)	9.5590(5)	17.290(1)	5.6256(5)	14.0839(8)
β (deg)	90	90.010(2)	90	90	90
V (Å^3)	1007.93(18)	503.81(5)	883.99(16)	469.20(7)	2793.6(5)
ρ_{calc} (g/cm^3)	4.288	4.289	3.480	3.976	4.089
λ (Å)			Mo Kα (0.71073)		
μ (mm^{-1})	15.858	15.863	10.905	19.528	15.707
crystal size (mm^3)	0.14 × 0.06 × 0.04	0.14 × 0.12 × 0.10	0.12 × 0.06 × 0.05	0.18 × 0.08 × 0.05	0.14 × 0.06 × 0.06
goodness of fit	1.206	1.101	1.427	1.120	1.122
R_1 ($I > 2\sigma(I)$)	0.0264	0.0278	0.0502	0.0486	0.0174
wR_2 (all data)	0.0489	0.0679	0.1012	0.1132	0.0420

[a]Twinning involves inversion, so Flack parameter cannot be determined. [b]Flack parameter = 0.50(6).

Table 3. Selected Interatomic Distances (Å) for (1)−(5)[a]

compound	(1)	(2)	(3)	(4)	(5)
Composition	$CsFeGeO_4$	$CsFeGeO_4$	$KFeGeO_4$	$Rb_{0.94}Cs_{0.06}FeGeO_4$	$CsFeGe_2O_6$
M(1)−O(5)	1.7773(7)		1.796(3)		
M(1)−O(2)	1.7908(17)	1.831(5)	1.794(5)	1.792(9)	1.758(3)
					1.768(3)
M(1)−O(1)	1.8021(15)	1.856(4)	1.805(5)	1.801(10)	1.781(3)
	1.8134(15)		1.809(6)	1.802(11)	1.787(3)
M(1)−O(4)		1.831(4)		1.799(5)	
M(1)−O(6)		1.837(4)			
M(2)−O(2)	1.7870(17)		1.796(5)	1.799(9)	
M(2)−O(4)	1.7947(9)		1.798(3)		
M(2)−O(5)		1.826(3)		1.778(4)	
M(2)−O(3)	1.8028(16)	1.835(4)	1.791(5)	1.789(8)	
	1.8047(16)		1.815(5)	1.804(9)	
M(2)−O(8)		1.856(5)			
M(2)−O(7)		1.861(5)			
Ge(1)−O(3)		1.751(4)			
Ge(1)−O(4)		1.754(4)			
Ge(1)−O(2)		1.764(4)			
Ge(1)−O(1)		1.769(5)			
Ge(2)−O(5)		1.732(3)			
Ge(2)−O(6)		1.752(4)			
Ge(2)−O(8)		1.753(4)			
Ge(2)−O(7)		1.772(5)			

[a]M = Fe for (2), and M = mixed Fe/Ge site for (1), (3), (4), and (5).

Ion exchange reactions were performed on (1) by layering 0.1 g of the sample under 1 g of the appropriate ANO_3 (A = K, Rb) flux in a fused-silica ampule measuring 7.5 cm in length. The tube containing the charge was heated for several hours. Once the reaction was complete, the flux was dissolved in hot water and the crystals were thoroughly rinsed with acetone and examined by single crystal X-ray diffraction. The specific amounts of the reagents and the flux used for the synthesis of all reported compositions, in addition to the heating and cooling cycle, are detailed in Table 1.

Solid State Synthesis. Polycrystalline samples of $CsFeGeO_4$ were synthesized by using Cs_2CO_3, Fe_2O_3, and elemental Ge powder in a stoichiometric ratio. The starting materials were thoroughly mixed in an agate mortar and pestle and then loaded into an alumina crucible that, prior to use, was thoroughly cleaned in aqua regia and dried in a drying oven. The charge was heated at 600 °C/h to 400 °C, maintained at this temperature for 16 h to decompose the carbonate, and then ramped at 600 °C/h to 650 °C, maintained at this temperature for 16 h whereupon the furnace was shut off and allowed to cool to room temperature. Additional intermittent grindings and heat treatments for 16 h at 900 °C led to the formation of a product consisting entirely of the desired stoichiometry, $CsFeGeO_4$ (6) however, as a mixture of the two polymorphs (1) and (2). One key observation is the necessity of using elemental Ge, which afforded only $CsFeGeO_4$, whereas the use of GeO_2 inevitably led to the formation of a small amount of a side product, $CsFeGe_2O_6$, in addition to $CsFeGeO_4$. This side product, $CsFeGe_2O_6$, was crystallized for structure determination and ultimately prepared

https://dx.doi.org/10.1021/acs.inorgchem.0c00936
Inorg. Chem. 2020, 59, 9699−9709

phase pure by heating stoichiometric amounts of $CsNO_3$, Fe_2O_3, and GeO_2 at 875 °C.

Single Crystal X-ray Diffraction (SCXRD). X-ray intensity data from suitable crystals of (**1**)−(**5**) were collected at 301(2) K using a Bruker D8 QUEST diffractometer equipped with a PHOTON 100 CMOS area detector and an Incoatec microfocus source (Mo Kα radiation, λ = 0.71073 Å).[22] The raw area detector data frames were reduced and corrected for absorption effects using the SAINT+ and SADABS programs.[22,23] Initial structural models were obtained with SHELXT.[24] Subsequent difference Fourier calculations and full-matrix least-squares refinement against F^2 were performed with SHELXL-2018 using the ShelXle interface.[25,26] Crystallographic and refinement data and interatomic distances for all compounds are listed in Tables 2 and 3, respectively. Additional crystallographic detail is provided in the Supporting Information (SI).

Powder X-ray Diffraction (PXRD). Phase purity of the compounds used for bulk property measurements was determined using a Bruker D2 Phaser equipped with an LYNXEYE silicon strip detector and Cu Kα radiation (Cu Kα radiation, λ = 1.5418 Å). The step-scan covered the angular range 10−70° in steps of 0.02°. The experimental and calculated PXRD patterns are provided in the SI.

Energy Dispersive Spectroscopy (EDS). Semiquantitative elemental analyses for (**1**)−(**5**) were carried out using a TESCAN Vega-3 SBU scanning electron microscope (SEM) with EDS capabilities. The crystals were mounted on carbon tape and the analysis was carried out using a 20 kV accelerating voltage and an accumulation time of 20 s. EDS verified the presence of the appropriate elements in all title compositions. Also, the absence of extraneous elements such as silver from the reaction vessel was confirmed within the detection limits of the instrument.

Optical Properties. UV−vis diffuse reflectance spectroscopy data were collected using a PerkinElmer Lambda 35 UV−vis scanning spectrophotometer equipped with an integrating sphere in the range of 200−900 nm. The reflectance data were converted to absorbance data using the Kubelka−Munk function.[27]

Magnetic Susceptibility. Magnetic properties were measured using a Quantum Design Magnetic Properties Measurement System (QD MPMS 3 SQUID Magnetometer). Magnetic susceptibility was measured under zero-field cooled (zfc) and field cooled (fc) conditions from 2 to 300 K in an applied field of 0.1 T. Magnetization as a function of field was measured from −5 to 5 T at 2 K. Data were corrected for sample shape and radial offset effects as described previously.[28] No differences were observed between the zfc and fc data; therefore, only the zfc data are provided.

Ferroelectric Measurement. Ferroelectric measurements were performed using a Radiant Technologies RT66A ferroelectric test system with a TREK high-voltage amplifier between 70 and 180 °C in a Delta 9023 environmental test chamber. The material was pressed into 12.5 mm diameter and 1 mm-thick pellet sintered at 1000 °C. Conducting silver paste was painted on both sides of the pellet surfaces for electrodes using a brush. A maximum voltage of 2000 V was applied to the sample. A detailed description of the methodology used has been published elsewhere.[29] To measure any possible ferroelectric behavior, the polarization was measured at room temperature using an alternating electric field of 2 kV/mm with frequencies of 1 to 1000 Hz. The temperature was allowed to stabilize before the polarization was measured.

Second Harmonic Generation (SHG). Powder SHG measurements were performed on a modified Kurtz nonlinear-optical (NLO) system using a pulsed Nd:YAG laser (Quantel Ultra 50) with a wavelength of 1064 nm. Comparisons with known SHG materials were made using ground crystalline α-SiO_2. A detailed description of the equipment and methodology has been published elsewhere. No index-matching material was used in any of the experiments.[30,31]

First-Principles Calculations. We performed first-principles calculations in the form of DFT, with an on-site Coulomb interaction, i.e., DFT+U, using the Vienna Ab-initio Package (VASP) code,[32,33] projector augmented wave (PAW) method,[34,35] and generalized gradient approximation of Perdew, Burke, and Ernzerhof (PBE).[36] To model the mixing and partial occupancies in the studied compounds, super quasi-random structures (SQSs) were made for (**1**)−(**4**). In the case of (**1**), we considered two possible orderings of the Fe and Ge atoms: (**1.1**) where Fe and Ge atoms are ordered along c-direction on Wyckoff positions (0.07820, 0.25957, 0.09318) and (0.40751, 0.2351, 0.15741), respectively; and (**1.2**) containing mixed Fe and Ge sites. For (**3**) and (**4**), we only considered completely mixed Fe/Ge sites, as in (**1.2**). Also, we should point out that for (**4**), we used the pure Rb analogue, $RbFeGeO_4$, as a model because the as synthesized compound, $Rb_{0.94}Cs_{0.06}FeGeO_4$, has a very low Cs concentration requiring very large SQS (>700 atoms) to reproduce. Because we aim to study the possibility of ion-exchange in (**1**), we also made pure K and Rb analogues of the (**1.2**) structure.

To see if the studied compounds are thermodynamically stable, i.e., if they break the A−Fe−Ge−O convex hull (A = K, Rb, Cs), their formation energies were compared with respect to Open Quantum Materials Database (OQMD).[37,38] For (**1**) and (**2**), we also compared their formation energies with respect to the Materials Project (MP) convex hull.[39] We used the following calculation set-ups; for the OQMD: 520 eV cutoff energy for the plane wave basis set, 10−4 eV energy convergence criterion, k-point mesh for (**1**) and (**3**) of 5 × 9 × 3, and for (**2**) and (**4**) 5 × 9 × 5, and U_{eff} = 4.0 eV for the Fe atoms; and for MP: 520 eV cutoff energy for the plane wave basis set, 4 × 10−4 eV energy convergence criterion, 3 × 5 × 2 and 3 × 5 × 3 k-point meshes for (**1**) and (**2**), respectively, and U_{eff} = 5.3 eV for the Fe atoms. We considered spin-polarization, with ferromagnetic (FM) and antiferromagnetic (AFM) (0 μ_B magnetic moment) ordering of the Fe atoms. The ground state geometry was obtained by relaxing the cell volume, cell shape and atomic positions. The adsorption indexes of (**1**) and (**2**) were obtained from the calculated frequency dependent dielectric function in the independent-particle picture.

RESULTS AND DISCUSSION

Flux and Solid State Synthesis. The purpose of flux crystal growth is normally to obtain high quality single crystals for structure determination, while solid state syntheses are typically used when large quantities of a material need to be

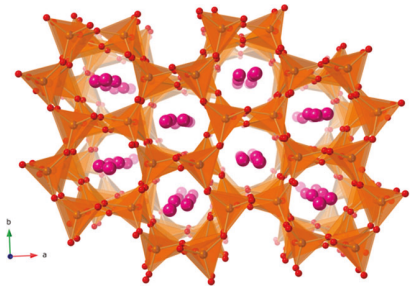

Figure 1. Crystal structure of (**1**) down the c-axis. Mixed Fe/Ge sites are shown in orange. Cs and O are shown as pink and red spheres, respectively.

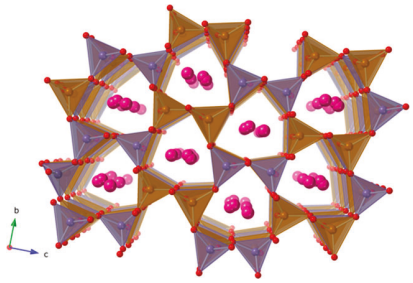

Figure 2. Polyhedral representation of (**2**) down the a-axis emphasizing the ordered FeO_4 and GeO_4 tetrahedra. Cs, Fe, Ge, and O are shown in pink, brown, purple, and red, respectively.

https://dx.doi.org/10.1021/acs.inorgchem.0c00936
Inorg. Chem. 2020, 59, 9699−9709

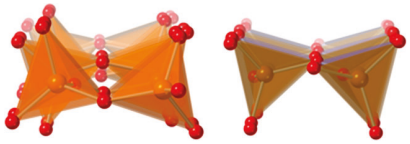

Figure 3. Depiction of distorted $(Fe/Ge)O_4$ tetrahedra in (**1**), shown on the left, compared to ordered FeO_4 and GeO_4 units in (**2**), shown on the right.

prepared. Since solid state reactions are carried out at temperatures high enough to enable the solid state diffusion of the reagents, they typically result in the thermodynamically most stable product. Flux reactions, on the other hand, are carried out at relatively lower temperatures and, hence, have the potential of resulting in kinetically stabilized phases. In addition, the identity of the products that crystallize in flux reactions can be subtly influenced by the reaction conditions, such as the flux to reagent ratio as well as by the particular flux chosen.

It is known that molten alkali halides containing one fluoride component demonstrate excellent capacity to dissolve a variety of oxides, in part because of the ability of the fluoride ion to act as a mineralizer.[40] For that reason, we explored mixed cesium chloride fluoride fluxes to crystallize new products in the Cs/Fe/Ge/O quaternary phase space in an attempt to target mixed iron germanium zeotypes. Using a 16:1 flux to reagent ratio by mass and employing a dwell time of 24 h, orthorhombic $CsFeGeO_4$ (**1**) can be crystallized. The structure of (**1**), as described in more detail later, consists of compositionally disordered corner sharing $(Fe,Ge)O_4$ tetrahedra that create channels in which the cesium cations reside. Using the same reaction temperature but decreasing the reaction time to 12 h and changing the flux to reagents ratio to a 9:1 by mass, monoclinic $CsFeGeO_4$ (**2**) can be crystallized. The structure of (**2**), exhibits an identical framework structure

Table 4. ΔH_{ie} (eV/atom) for Exchanging Cs with K or Rb in $CsFeGeO_4$, Using Different Salts As Reactants

	salts		
A	ANO_3	AF	ACl
K	0.0260	0.0417	0.0213
Rb	−0.0778	−0.0912	−0.1014

to (**1**), albeit featuring ordered FeO_4 and GeO_4 tetrahedra, as described in more detail later. $CsFeGeO_4$ bears structural similarities with a family of pnictates, several members of which crystallize in the monoclinic $P2_1$ space group, including $AZnPO_4$ (A = Rb, NH_4),[18,19] $KCuPO_4$,[20] and $TlZnAsO_4$.[21]

This change in product outcome due to changes in time and flux to reagent ratio suggests that the disordered orthorhombic polymorph is favored over the ordered monoclinic polymorph when the dissolution of the starting reagents is enhanced by lengthening the dwell time and by increasing the amount of flux. Single crystals of (**2**) of suitable size for crystal picking were grown by layering 1 mmol of FeF_3 and 1 mmol of GeO_2 under 0.93 g of CsCl and 0.84 g of CsF. Notice that CsCl-CsF eutectic was not used in this case. Although numerous flux crystal growth conditions were tried, none resulted in the formation of a product consisting of a single phase of (**1**).

To determine if a pure phase of (**1**) could be obtained by other routes, the solid state synthesis of (**1**) was attempted by heating a stoichiometric mixture of Cs_2CO_3, Fe_2O_3 and GeO_2; however, this always resulted in the presence of an impurity phase, $CsFeGe_2O_6$, that we subsequently synthesized both as single crystal for structure determination and as a polycrystalline powder for physical property measurements. Somewhat surprisingly, the synthesis route that resulted in phase pure $CsFeGeO_4$ consisted of heating a stoichiometric mixture of Cs_2CO_3, Fe_2O_3 and Ge; changing the Ge source from GeO_2 to elemental Ge afforded "phase pure" $CsFeGeO_4$ (**6**). However,

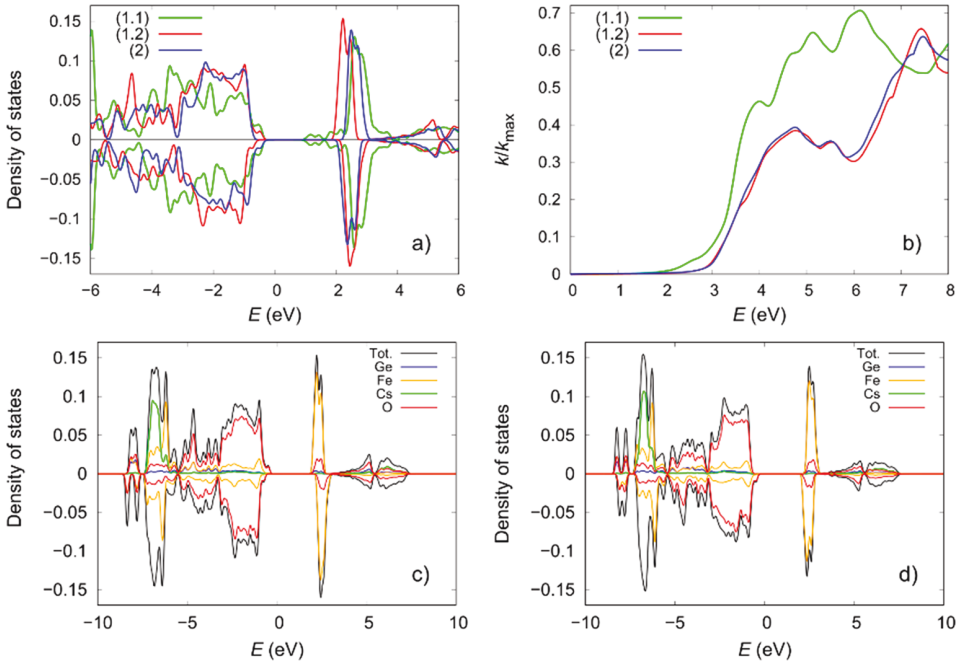

Figure 4. (a) Density of states (DOS) and (b) adsorption indexes of (**1.1**), (**1.2**), and (**2**) in the AFM state. Projected DOS (PDOS) of (c) (**1.2**) and (d) (**2**) in the AFM state. The positive and negative PDOS show the spin-up and spin-down channels, respectively.

https://dx.doi.org/10.1021/acs.inorgchem.0c00936
Inorg. Chem. 2020, 59, 9699−9709

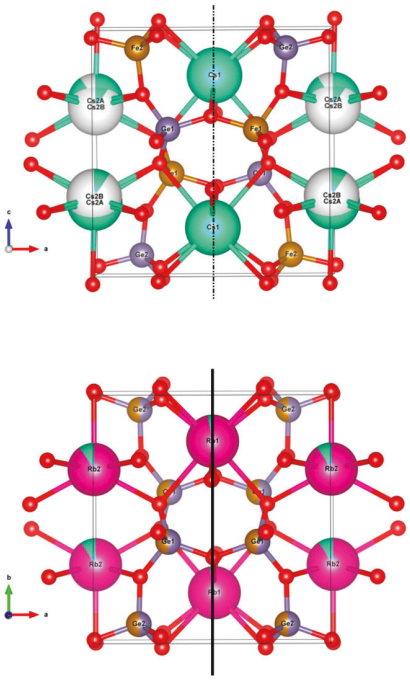

Figure 5. Comparison of the crystal structures of (**2**) and (**4**). Ordering of the Fe and Ge atoms in (**2**), shown at the top makes Fe and Ge sites inequivalent and inconsistent with mirror symmetry. This allows for its monoclinic $P2_1$ symmetry. In contrast, 50/50 disorder of all Fe/Ge sites in (**4**), shown at the bottom, renders Fe(1)/Ge(1) and Fe(2)/Ge(2) sites equivalent, and therefore related by a mirror plane symmetry (vertical heavy black line). This allows for the orthorhombic $Pmc2_1$ crystal symmetry for (**4**).

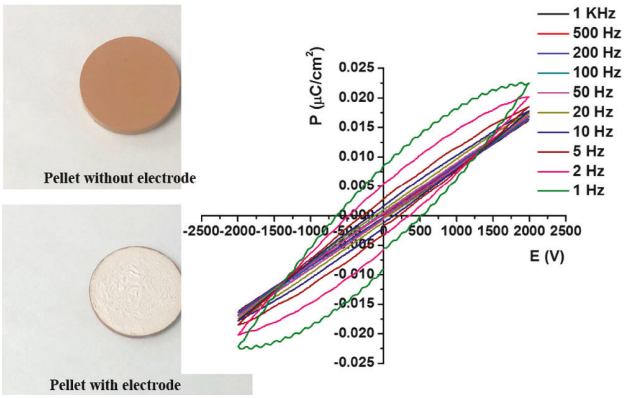

Figure 6. Frequency-dependent polarization measurements for (**6**). The measured polarization loops are not ferroelectric hysteresis loops but are a result of dielectric loss in the material.

due to the virtually identical PXRD patterns of (**1**) and (**2**), it is extremely challenging to determine the presence or absence of both (**1**) and (**2**) in the sample. The presence of a trace amount of the acentric polymorph (**2**) in (**6**) was verified by SHG measurements as it had an SHG activity of 0.25 times of α-SiO_2. The simultaneous formation of both $CsFeGeO_4$ polymorphs, via the conventional solid state route, is in excellent agreement with the DFT calculations, vide infra, which predicted both phases to be energetically stable with a miniscule energy difference.

Crystal Structures. The disordered $CsFeGeO_4$ polymorph, (**1**), crystallizes in the centrosymmetric orthorhombic space group *Pbcm* with lattice parameters a = 9.5617(9) Å, b = 5.6785(6) Å, c = 18.5636(19) Å, and V = 1007.93(18) Å^3. The asymmetric unit for (**1**) consists of two cesium atoms, two mixed Fe/Ge sites and five unique oxygen atoms. The Fe/Ge(1) is coordinated to two O(1), O(2), and O(5) with bond lengths of 1.8021(15), 1.8134(15), 1.7908(17), and 1.7773(7) Å, respectively. The Fe/Ge(2) is coordinated to O(2), two O(3) and O(4) with bond lengths of 1.7870(17), 1.8028(16), 1.8047(16), and 1.7947(9) Å, respectively. These are in reasonable agreement with the Fe−O distances for (**2**) considering site mixing with Ge. Structurally, (**1**) consists of corner-sharing $(Fe/Ge)O_4$ framework with large eight-sided channels running down the *b*-axis. These are occupied by the cesium ions which provide charge balance to the anionic $[FeGeO_4]^-$ framework. Figure 1 shows the polyhedral representation of (**1**).

The ordered $CsFeGeO_4$ polymorph, (**2**), crystallizes in the acentric monoclinic space group $P2_1$ with lattice parameters a = 9.2751(5) Å, b = 5.6825(3) Å, c = 9.5590(5) Å, β = 90.010(2)°, and V = 503.81(5) Å^3. The asymmetric unit cell consists of two cesium atoms, two germanium atoms, two iron atoms, and eight oxygen atoms. Fe(1) is coordinated to O(1), O(2), O(4), and O(6) in a tetrahedral environment with bond lengths of 1.8564, 1.831(5), 1.831(4), and 1.837(4) Å, respectively. A similar tetrahedral environment is exhibited by Fe(2), which is coordinated to O(3), O(5), O(7), and O(8) with bond lengths 1.835(4), 1.826(3), 1.861(5), and 1.856(5) Å, respectively. These bond lengths are in fair agreement with the Fe−O bond lengths ranging from 1.828 Å−1.896 Å in $Ba_4KFe_3O_9$,[41] which contains discrete 6-membered rings of corner-sharing FeO_4 tetrahedra, as well as other compounds containing iron in tetrahedral, noncentrosymmetric environment.[11,16] Structurally related to (**1**), (**2**) also comprises large tunnels that crisscross the crystal structure along the *a*-, *b*-, and *c*-axis; eight-, four-, and six-ring channels run along the *a*-, *b*-, and *c*-axis, respectively, and are occupied by the monovalent cesium ions that provide charge balance for the three-dimensional anionic $[FeGeO_4]^-$ framework. Figure 2 illustrates the crystal structure of (**2**).

The unit cell volume of (**1**) is twice that of the ordered polymorph, (**2**), because the *c*-axis, corresponding to the *a*-axis in the monoclinic form, has doubled. The most likely reason for this is the distortion in the $(Fe,Ge)O_4$ tetrahedra. Figure 3 shows the distortion of $(Fe/Ge)O_4$ network in (**1**) relative to ordered FeO_4 and GeO_4 network in (**2**).

Stability of (1) and (2). To better understand the existence of the two polymorphs (**1**) and (**2**), we performed DFT calculations. For each of the studied structures, we calculated their ΔH_f and stability—the distance from the respective convex hull. Shown in Table 6 are the ΔH_f and stabilities for (**1.1**), (**1.2**), and (**2**) compounds, calculated using the OQMD and MP calculation setup. Evidently, both (**1**) and (**2**) are thermodynamically stable, i.e., they break both OQMD and MP convex hull. The orthorhombic polymorph, (**1.2**) is more stable, has more negative ΔH_f by 45.2 meV/atom, than (**1.1**), indicating that complete mixing is preferred over ordering on the Fe/Ge sites in (**1**). The AFM systems are more stable compared to the FM systems for each of the polymorphs. Also, it is worth noticing that (**2**) is more stable compared to (**1.2**) by 1 meV. This minimal energy difference potentially explains why (**1**) and (**2**) form simultaneously via the solid state route.

https://dx.doi.org/10.1021/acs.inorgchem.0c00936
Inorg. Chem. 2020, 59, 9699−9709

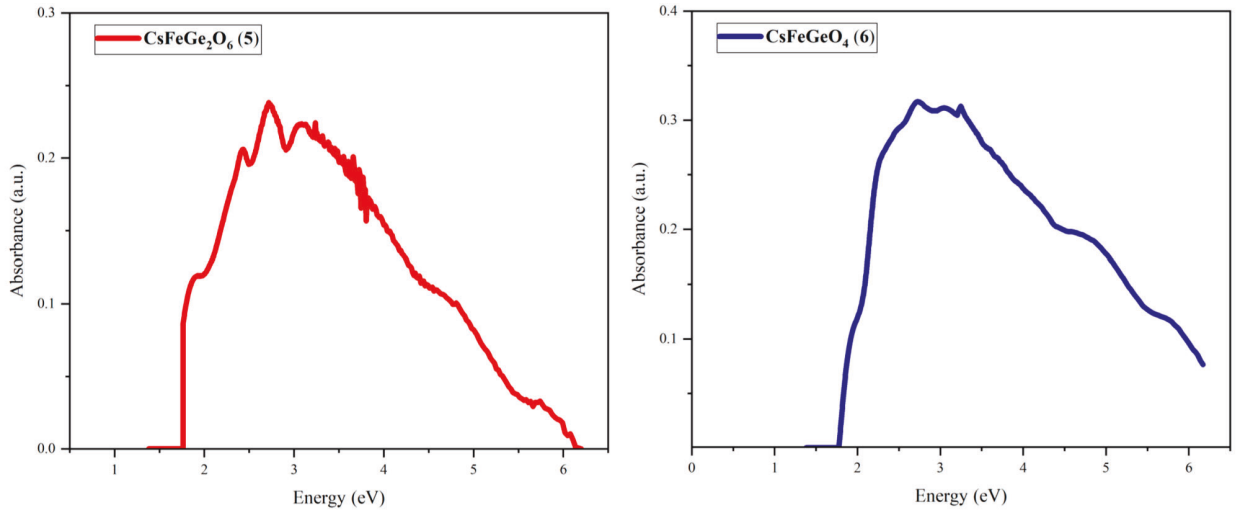

Figure 7. UV−vis plots for (**5**) (left) and (**6**) (right).

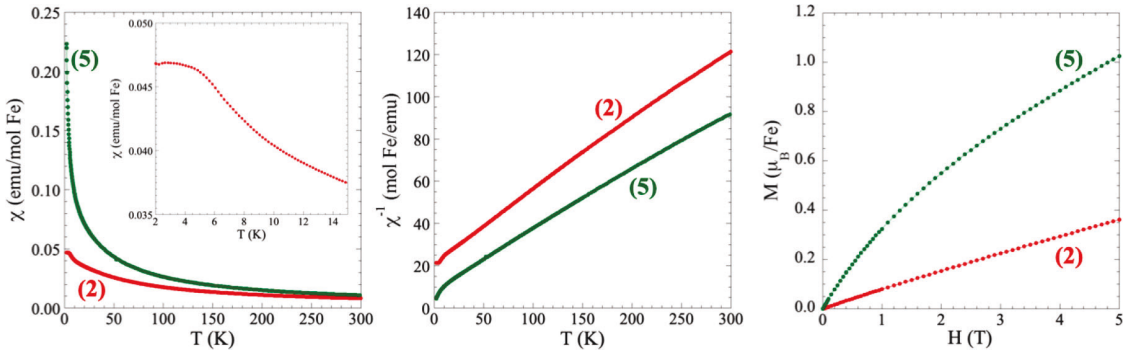

Figure 8. Magnetic susceptibility, inverse susceptibility, and magnetization as a function of field for compounds (**2**) and (**5**) measured in an applied field of H = 0.1 T and at T = 2 K, respectively.

Table 5. Magnetic Properties for (2) and (5) at H = 0.1 T

compound	fit range (K)	μ_{eff} (μ_B/M)	μ_{calc} (μ_B/M)	θ (K)
(**2**)	50−300	4.90(2)	5.92	−69.9(10)
(**5**)	50−300	5.37(2)	5.92	−36.6(6)

In addition to studying the stability of the different polymorphs, we also analyzed the electronic and optical properties of (**1**) and (**2**). Shown in Figure 4 are density of states (DOS), the projected DOS (PDOS), and adsorption indexes of (**1.1**), (**1.2**), and (**2**) in AFM systems, the lower energy phase. The DOS, PDOS, and adsorption indexes of the polymorphs in FM state are given in Figure S6. It is noticeable that the DOS of (**1.1**) are significantly different from the DOS of (**1.2**) and (**2**) (Figure 4a), with states extending from the conduction band into the band gap. The adsorption indexes (Figure 4b) reflect the DOS, with sharp increase in adsorption starting from the band gap energy, as well as significant difference between the adsorption index of (**1.1**) and the ones of (**1.2**) and (**2**). Considering the difference in the DOS and adsorption indexes, and the fact that (**1.1**) is less stable than (1.2), in the continuation we are only going to discuss the

Table 6. Formation Energies, ΔH_f (eV/atom), and Stabilities (Distance from the Convex Hull), (eV/atom), Calculated Using OQMD and MP Calculation Setup[a]

	(1.1)		(1.2)		(2)	
OQMD	ΔH_f	stability	ΔH_f	stability	ΔH_f	stability
FM	−1.8385	−0.0625	−1.9336	−0.1576	−1.9335	−0.1575
AFM	−1.8892	−0.1132	−1.9344	−0.1584	−1.9357	−0.1597
AFM-FM	−0.0506		−0.0007		−0.0021	
MP	ΔH_f	stability	ΔH_f	stability	ΔH_f	stability
FM	−2.0127	−0.0017	−2.0873	−0.0763	−2.087	−0.076
AFM	−2.0355	−0.0245	−2.0877	−0.0767	−2.088	−0.077
AFM-FM	−0.0227		−0.0004		−0.0008	

[a]Negative stabilities indicate that the compound's ΔH_f is below the Cs−Fe−Ge-O convex hull.

https://dx.doi.org/10.1021/acs.inorgchem.0c00936
Inorg. Chem. 2020, 59, 9699−9709

results for (**1.2**), referring to it as polymorph (**1**). PDOS of (**1.1**) are shown in Figure S7. Both (**1**) and (**2**) polymorphs have clearly defined band gaps, with (**1**) in FM and AFM ordering having band gaps of 2.62 and 2.48, respectively, and (**2**) in FM and AFM ordering having band gaps of 2.96 and 2.61, respectively. It is also worth noticing that the largest contribution to the top of valence band come from O states, while the largest contribution to the bottom of the conduction band comes from the Fe states. This is the case for both (**1**) and (**2**) and for the AFM and FM systems. Such distribution of states around the band gap indicates that the $CsFeGeO_4$ compound is a charge transfer semiconductor.

Ion Exchange. To investigate the possibility of exchanging Cs with other alkali ions, such as Rb and K, we initially calculated the ion exchange energies using DFT. Assuming that solid state synthesis can be carried out, we focused on ion exchange reactions in the melt, i.e.,

$$CsFeGeO_4 + AX = AFeGeO_4 + CsX$$

where AX is the salt, in this case ANO_3, AF, and ACl, with A = K, Rb, and $AFeGeO_4$ with the same structure as (**1.2**), as noted previously. The ion exchange energies, ΔH_{ie}, are calculated using the equation:

$$\Delta H_{ie} = [\Delta H_f(AFeGeO_4) + \Delta H_f(CsX) - \Delta H_f(CsFeGeO_4) - \Delta H_f(AX)]/N$$

where $\Delta H_f(AFeGeO_4)$, $\Delta H_f(CsX)$, $\Delta H_f(CsFeGeO_4)$, and $\Delta H_f(AX)$ are the calculated formation energies, per formula unit, of $AFeGeO_4$, CsX, $CsFeGeO_4$, and AX, respectively, and N is the total number of atoms participating in the reaction. Shown in Table 4 are the calculated ΔH_{ie} using ANO_3, AF, and ACl salts as references. Evidently, the ΔH_{ie} are negative for the Cs/Rb ion exchange reaction regardless of the reactant salt, indicating that this reaction is thermodynamically favorable. In the case of the Cs/K ion exchange reaction, the ΔH_{ie} are positive, but ΔH_{ie} values are very small, such as a small increase in temperature, i.e., 29, 211, and −26 °C for ANO_3, AF, and ACl, respectively, could promote the formation of the $KFeGeO_4$ compound.

DFT calculations, using alkali nitrates as a reference, (because nitrate salts have lower melting points than the halide salts, they were used for the ion exchange experiments) indicated that (**1**) could afford $KFeGeO_4$ and $RbFeGeO_4$ from the respective molten nitrates. To validate the DFT results, crystals of (**1**) were soaked in molten KNO_3 and $RbNO_3$ at 375 and 350 °C, respectively, for 16 h, followed by extensive material characterization. The crystals shape was retained during the soaking process, prompting us to perform single crystal X-ray diffraction. The structure determination confirmed that this process was a single-crystal to single-crystal ion exchange process, resulting in stoichiometric $KFeGeO_4$ (**3**) and mixed Rb/Cs $Rb_{0.94}Cs_{0.06}FeGeO_4$ (**4**). Two control experiments were performed to ensure that (**3**) and (**4**) did not result from dissolution and recrystallization in the molten nitrate salt environment, but rather resulted from the ion exchange process. First, Fe_2O_3 and GeO_2 were heated in molten KNO_3, and second, presynthesized $KFeGeO_4$ powder was heated in molten KNO_3. Both reactions were held at 375 °C for 16 h. In the first case, the only products were the unreacted Fe_2O_3 and GeO_2 as confirmed by the PXRD. In the second experiment only the parent $KFeGeO_4$ powder, but no crystals, was observed. These results corroborate that the process is indeed a single-crystal to single-crystal ion exchange process. $KFeGeO_4$ (**3**) crystallizes in orthorhombic space group *Pbcm*, is analogous to (**1**), and is also a polymorph of hexagonal $KFeGeO_4$, which crystallizes in space group $P6_3$, previously reported by Hammond et al.[12] (**3**) could not be obtained using high temperature molten salt synthesis methods nor via the solid state route, as this always led to the formation of hexagonal $KFeGeO_4$. From these empirical results, it can be deduced that the hexagonal and orthorhombic phases are the thermodynamically and kinetically stabilized $KFeGeO_4$ polymorphs, respectively. This was further elaborated and quantified by the first-principles calculations which indicate that in the case of the $KFeGeO_4$ polymorphs, the hexagonal polymorph is more stable by 13.5 meV/atom than the orthorhombic (**3**)—the polymorph derived from ion exchange on (**1.2**). This shows that the hexagonal polymorph is thermodynamically favored, while the formation of (**3**) can only be achieved kinetically.

In the ion exchange experiments carried out for (**1**), the orthorhombic crystal symmetry is preserved upon its single-crystal to single-crystal ion exchange transformation to $KFeGeO_4$ (**3**) and $Rb_{0.94}Cs_{0.06}FeGeO_4$ (**4**); however, (**4**) crystallizes in space group $Pmc2_1$ rather than in the *Pbcm* space group of the parent (**1**). Both (**3**) and (**4**), similar to (**1**), exhibit two mixed, statistically disorder Fe/Ge sites and are structurally identical to (**1**). A brief comparison of the crystal structures of (**2**) and (**4**) is provided in Figure 5.

Second Harmonic Generation (SHG). All materials that crystallize in one of the noncentrosymmetric crystal classes, except 432, may exhibit SHG behavior, where large SHG efficiency is typically correlated with large dipole moments.[42−44] (**2**) was observed to be SHG active with an efficiency of 1.5 times of α-SiO_2, hence confirming its acentric space group $P2_1$. (**5**) was found to be SHG active with an efficiency of 0.4 times of α-SiO_2. This confirmed its acentric cubic space group *I*-43*d*. Prior to this work, $CsFeGe_2O_6$ was reported to crystallize in centric cubic space group *Ia*-3*d* based on an analysis of powder diffraction data.[45] Polycrystalline $CsFeGeO_4$ (**6**), prepared via solid state synthesis, displayed a weak SHG signal with an intensity of 0.25 times of α-SiO_2. This verified the presence of a trace amount of the acentric monoclinic $CsFeGeO_4$ polymorph (**2**) in (**6**). For all three materials, the most likely reason for a small SHG efficiency could be attributed to a small dipole moment. Large SHG efficiencies are typically associated with large intrinsic dipole moment of the material.

Polarization Measurements (Ferroelectricity). Although polycrystalline $CsFeGeO_4$ (**6**) exhibits a small local dipole moment as indicated by a small SHG coefficient, it was nevertheless measured for its macroscopic polarity by checking to establish whether or not it displayed ferroelectric behavior. If a material is indeed ferroelectric, its polarity must be reversed under an externally applied electric field. Because of the strong frequency dependence of the ferroelectricity of any material, the polarization measurements have to be carried out at several different frequencies. The "banana-shaped" or "fat" loops observed for (**6**), as shown in Figure 6, are not precisely ferroelectric hysteresis loops but are potentially the result of dielectric loss.[46] It can be inferred from these loops that the material is incapable of reversing its polarity under applied electric field. The absence of ferroelectric property in the material can be rationalized on the basis of the local coordination of the Fe atoms, which in this case are

https://dx.doi.org/10.1021/acs.inorgchem.0c00936
Inorg. Chem. 2020, 59, 9699−9709

tetrahedrally coordinated, and hence their contribution to macroscopic polarity is almost negligible. This can be construed along the lines of what was observed in case of cesium vanadate, $Cs_2V_3O_8$, which contains VO_4 and VO_5 polyhedra.[47] Although $Cs_2V_3O_8$ crystallizes in the non-centrosymmetric polar space group *P4bm*, it does not display ferroelectric behavior, likely for two reasons. First, the contribution to macroscopic polarity by the VO_4 polyhedra is much less because of their tetrahedral geometry, and second and more importantly, the physical displacement of VO_5 polyhedra along the *c*-axis was energetically unfavorable which would otherwise be one way for the dipole moment reversal in the material. As opposed to this, materials that are well-known for their large ferroelectric responses, such as $BaTiO_3$ and $KNbO_3$, the ferroelectric behavior arises due to the polarization reversal involving physical displacement of the octahedrally coordinated metal species, Ti^{4+} in $BaTiO_3$ and Nb^{5+} in $KNbO_3$.[48,49]

Optical Properties. The UV−vis absorption spectra for (**5**) and (**6**) are shown in Figure 7. The band gaps for (**5**) and (**6**) are roughly the same, and based on extrapolations of the data shown and from Tauc plots, their band gaps fall into the range of 1.8 and 2.2 eV.[50] These band gaps are consistent with the yellowish-brown appearance of the materials indicating that they mostly absorb in the blue green (500−560 nm or 2.20−2.48 eV) region of the visible light spectrum. Additionally, these values are consistent with the optical band gap for Fe_2O_3 (E_g = ∼2.10 eV)[51] and other complex iron containing oxides, all of which have orange to reddish-brown appearance.[52,53]

Magnetic Properties. The temperature and field dependent magnetic properties for (**2**) and (**5**) are provided in Figure 8, and the magnetic data are summarized in Table 5. Both compounds obey the Curie−Weiss law for $T > 10$ K. A downturn in the susceptibility of (**2**) at $T = 2.6$ K is indicative of antiferromagnetic ordering. Fitting the magnetic susceptibility from 50 to 300 K afforded effective moments of 4.90(2) μ_B/Fe and 5.37(2) μ_B/Fe for (**2**) and (**5**), respectively. Although smaller than the calculated moment of 5.92 μ_B/Fe for free high spin Fe^{3+}, the effective moment of (**2**) is consistent with the magnetic moments usually observed for Fe^{3+} in tetrahedral coordination environment. It is usual to observe low and, at times, unusually low magnetic moments in complex iron based oxides that feature tetrahedral Fe^{3+}. For instance, Zhao et al. reported a magnetic moment of ∼3.933 μ_B/Fe for $Ba_4KFe_3O_9$,[42] which indicated the presence of antiferromagnetic interactions between Fe^{3+} ions within the Fe_6O_{18} rings making up the crystal structure; however, no antiferromagnetic transition was observed in the magnetic data and the compound was paramagnetic in the entire 2−400 K range. Similarly, the magnetic moments reported for tetrahedral Fe (III) in $BaFe_4O_7$ and $K_{0.22}Ba_{0.89}Fe_4O_7$ are 3.8(0.3) μ_B/Fe and 4.4(0.4) μ_B/Fe, respectively.[54] Also, low magnetic moments for tetrahedral Fe (III) determined from neutron diffraction studies are not uncommon and considered to arise from the partially covalent nature of the metal−oxygen bonds.[55,56] Low magnetic moments have also been observed for octahedral iron, for example in the pyroxene $Na_{0.5}Li_{0.5}FeGe_2O_6$ which has an observed moment of 4.5 μ_B/Fe.[57] The field dependent magnetizations for the two compounds are shown in Figure 8. No saturation is observed up to 5 T.

CONCLUSION

Two polymorphs of a new cesium ferrogermanate, $CsFeGeO_4$, crystallizing in the orthorhombic and monoclinic space groups *Pbcm* and $P2_1$ were grown out of mixed CsCl-CsF flux, and their structures were determined using single crystal X-ray diffraction. Molten alkali nitrate ion exchange experiments were carried out using the orthorhombic polymorph to yield $KFeGeO_4$ and $Rb_{0.94}Cs_{0.06}FeGeO_4$ as ion exchange products, as predicted by the DFT calculations. The materials were further characterized by SQUID magnetometry and UV−vis spectroscopy. First-principles calculations were carried out to elucidate the stability of the two polymorphs and to calculate their electronic and magnetic properties.

ASSOCIATED CONTENT

Supporting Information

The Supporting Information is available free of charge at https://pubs.acs.org/doi/10.1021/acs.inorgchem.0c00936.

Single crystal and polycrystalline powder optical images, PXRD patterns, EDS results, PDOS figures, and an extensive crystallographic refinement discussion (PDF)

Accession Codes

CCDC 1906065, 1906061, and 1959753−1959755 contain the supplementary crystallographic information for this paper. These data can be obtained free of charge via www.ccdc.cam.ac.uk/data_request/cif, or by emailing data_request@ccdc.cam.ac.uk, or by contacting The Cambridge Crystallographic Data Centre, 12 Union Road, Cambridge CB2 1EZ, UK; fax: +44 1223 336033.

AUTHOR INFORMATION

Corresponding Author

Hans-Conrad zur Loye − *Department of Chemistry and Biochemistry, University of South Carolina, Columbia, South Carolina 29208, United States;* orcid.org/0000-0001-7351-9098; Email: zurloye@mailbox.sc.edu

Authors

Mohammad Usman − *Department of Chemistry and Biochemistry, University of South Carolina, Columbia, South Carolina 29208, United States*

Vancho Kocevski − *Department of Mechanical Engineering, University of South Carolina, Columbia, South Carolina 29208, United States;* orcid.org/0000-0002-2127-5834

Mark D. Smith − *Department of Chemistry and Biochemistry, University of South Carolina, Columbia, South Carolina 29208, United States*

Gregory Morrison − *Department of Chemistry and Biochemistry, University of South Carolina, Columbia, South Carolina 29208, United States;* orcid.org/0000-0001-9674-9224

Weiguo Zhang − *Department of Chemistry, University of Houston, Houston, Texas 77204, United States*

Theodore Besmann − *Department of Mechanical Engineering, University of South Carolina, Columbia, South Carolina 29208, United States*

P. Shiv. Halasyamani − *Department of Chemistry, University of Houston, Houston, Texas 77204, United States;* orcid.org/0000-0003-1787-1040

Complete contact information is available at: https://pubs.acs.org/10.1021/acs.inorgchem.0c00936

https://dx.doi.org/10.1021/acs.inorgchem.0c00936
Inorg. Chem. 2020, 59, 9699−9709

Notes

The authors declare no competing financial interest.

■ ACKNOWLEDGMENTS

The syntheses, single crystal X-ray structural characterization, and magnetic measurements were carried out by M.U., M.D.S., G.M., and H.Z.L. who gratefully acknowledge the U.S. National Science Foundation for supporting this research through grant OIA-1655740. The SHG and polarization work was performed at the University of Houston, and W.Z. and P.S.H. thank the Welch Foundation (Grant E-1457) for support. V.K. and T.B. acknowledge the support by the U.S. Department of Energy, Office of Science, Basic Energy Sciences, under Award No. DE-SC0016574 (Center for Hierarchical Waste Form Materials). This research used computational resources provided by the National Energy Research Scientific Computing Center (NERSC) and the HPC cluster Hyperion, supported by The Division of Information Technology at the University of South Carolina.

■ REFERENCES

(1) Weckhuysen, B. M.; Yu, J. Recent Advances in Zeolite Chemistry and Catalysis. *Chem. Soc. Rev.* **2015**, *44*, 7022−7024.
(2) Song, Z.; Huang, Y.; Wang, L.; Li, S.; Yu, M. Composite 5A Zeolite with Ultrathin Porous TiO_2 Coating for Selective Gas Adsorption. *Chem. Commun.* **2015**, *51*, 373−375.
(3) Yang, H.; Luo, M.; Luo, L.; Wang, H.; Hu, D.; Lin, J.; Wang, X.; Wang, Y.; Wang, S.; Bu, X.; Feng, P.; Wu, T. Highly Selective and Rapid Uptake of Radionuclide Cesium Based on Robust Zeolitic Chalcogenide via Stepwise Ion-Exchange Strategy. *Chem. Mater.* **2016**, *28*, 8774−8780.
(4) Borade, R. B.; Clearfield, A. Synthesis of an Iron Silicate with the Ferrierite Structure. *Chem. Commun.* **1996**, *19*, 2267−2268.
(5) Joshi, P. N.; Awate, S. V.; Shiralkar, V. P. Partial Isomorphous Substitution of Fe^{3+} in the LTL Framework. *J. Phys. Chem.* **1993**, *97*, 9749−9753.
(6) Vaughan, D. E. W.; Strohmaier, K. G.; Pickering, I. J.; George, G. N. Transition Metal Framework Substitutions in Sodalites. *Solid State Ionics* **1992**, *53*−*56*, 1282−1291.
(7) Latshaw, A. M.; Chance, W. M.; Morrison, G.; zur Loye, K. D.; Wilkins, B. O.; Smith, M. D.; Whitfield, P. S.; Kirkham, M. J.; Stoian, S. A.; zur Loye, H.-C. Synthesis of a Ferrolite: A Zeolitic All-Iron Framework. *Angew. Chem., Int. Ed.* **2016**, *55* (42), 13195−13199.
(8) Cameron, M.; Papike, J. J. Structural and Chemical Variations in Pyroxenes. *Am. Mineral.* **1981**, *66*, 1−50.
(9) Faust, G. T. The Fusion Relations of Iron-Orthoclase. *Am. Mineral.* **1936**, *21*, 735−763.
(10) Bentzen, J. J. Three Crystalline Polymorphs of $KFeSiO_4$, Potassium Ferrisilicate. *J. Am. Ceram. Soc.* **1983**, *66*, 475−479.
(11) Henry, P. F.; Weller, M. T. $CsFeSiO_4$: a maximum iron content zeotype. *Chem. Commun.* **1998**, *24*, 2723−2724.
(12) Hammond, R.; Barbier, J. Low-temperature $KFeGeO_4$. *Acta Crystallogr., Sect. C: Cryst. Struct. Commun.* **1999**, *55*, IUC9900074.
(13) Lévy, D.; Barbier, J. A Sanidine Feldspar Analogue: $KFeGe_3O_8$. *Acta Crystallogr., Sect. C: Cryst. Struct. Commun.* **1998**, *54*, IUC9800043.
(14) Mwamuka, J. N.; Gemmill, W. R.; Stitzer, K. E.; Smith, M. D.; zur Loye, H.-C. Crystal Growth of New Strontium Iron Rhodium Oxides: $Sr_4Fe_{0.73}Rh_{2.27}O_9$ and $SrFe_{0.71}Rh_{0.29}O_3$. *J. Alloys Compd.* **2004**, *377*, 91−97.
(15) Gemmill, W. R.; Smith, M. D.; zur Loye, H.-C. Synthesis and Structural Characterization of Two New Hexagonal Osmates: $Ba_2Fe_{0.92}Os_{1.08}O_6$ and $Ba_2Co_{0.77}Os_{1.23}O_6$. *Solid State Sci.* **2007**, *9*, 380−384.
(16) Roof, I. P.; Smith, M. D.; zur Loye, H.-C. Crystal Growth of a New Series of Non-Centrosymmetric Oxides, Ln_3FeO_6 (Ln = La, Nd, Sm, Eu and Gd). *Solid State Sci.* **2010**, *12*, 1211−1214.
(17) Giaquinta, D. M.; Papaefthymiou, G. C.; zur Loye, H.-C. Structural and Magnetic Studies of $Bi_2Fe_{4-x}Al_xO_9$. *J. Solid State Chem.* **1995**, *114*, 199−205.
(18) Elammari, L.; Elouadi, B. Structure Cristalline de $RbZnPO_4$. *J. Chim. Phys. Phys.-Chim. Biol.* **1991**, *88*, 1969−1974.
(19) Averbuch-Pouchot, M. T.; Durif, A. Donnees Cristallographiques sur les Deux Varietes du Phosphate Ammoniaco-Zincique: $ZnNH_4PO_4$. *Mater. Res. Bull.* **1968**, *3*, 719−722.
(20) Shoemaker, G. L.; Kostiner, E.; Anderson, J. B. The Crystal Structure of Potassium Copper(II) Phosphate $KCuPO_4$, an Example of a Three-Dimensional Network. *Z. Kristallogr.* **1980**, *152*, 317−332.
(21) Andratschke, M. Struktur und Eigenschaften von $TlZnPO_4$ und $TlZnAsO_4$. *Z. Anorg. Allg. Chem.* **1994**, *620*, 361−365.
(22) *APEX3*, version 2016.5-0; *SAINT+*, version 8.37A; Bruker AXS, Inc., Madison, Wisconsin, USA, 2016.
(23) SADABS-2016/2: Krause, L.; Herbst-Irmer, R.; Sheldrick, G. M.; Stalke, D. *J. Appl. Crystallogr.* **2015**, *48* (48), 3−10.
(24) (a) SHELXT: Sheldrick, G. M. Integrated Space-group and Crystal-structure Determination. *Acta Crystallogr., Sect. A: Found. Adv.* **2015**, *A71*, 3−8. (b) SHELXL: Sheldrick, G. M. Crystal Structure Refinement with SHELXL. *Acta Crystallogr., Sect. C: Struct. Chem.* **2015**, *C71*, 3−8.
(25) ShelXle: a Qt graphical user interface for SHELXL. Hübschle, C. B.; Sheldrick, G. M.; Bittrich, B. ShelXle: A Qt Graphical User Interface for SHELXL. *J. Appl. Crystallogr.* **2011**, *44*, 1281−1284.
(26) (a) LePage, Y. Computer Derivation of the Symmetry Elements Implied in a Structure Description. *J. Appl. Crystallogr.* **1987**, *20*, 264−269. (b) Spek, A. L. LEPAGE − An MS-DOS Program for the Determination of the Metrical Symmetry of a Translation Lattice. *J. Appl. Crystallogr.* **1988**, *21*, 578−579. (c) Spek, A. L. PLATON, An Integrated Tool for the Analysis of the Results of a Single Crystal Structure Determination. *Acta Crystallogr., Sect. A* **1990**, *A46*, C34. (d) PLATON: Spek, A. L. Structure Validation in Chemical Crystallography. *Acta Crystallogr., Sect. D: Biol. Crystallogr.* **2009**, *D65*, 148−155.
(27) Kubelka, P.; Munk, F. Ein Beitrag zur Optik der Farbanstriche. *Z. Technol. Phys.* **1931**, *12*, 593.
(28) Morrison, G.; zur Loye, H.-C. Simple Correction for the Sample Shape and Radial Offset Effects on SQUID Magnetometers: Magnetic Measurements on Ln_2O_3 (Ln = Gd, Dy, Er) standards. *J. Solid State Chem.* **2015**, *221*, 334−337.
(29) Ok, K. M.; Chi, E. O.; Halasyamani, P. S. Bulk Characterization Methods for Non-Centrosymmetric Materials: Second-harmonic Generation, Piezoelectricity, Pyroelectricity, and Ferroelectricity. *Chem. Soc. Rev.* **2006**, *35*, 710−717.
(30) Kurtz, S. K.; Perry, T. T. A Powder Technique for the Evaluation of Nonlinear Optical Materials. *J. Appl. Phys.* **1968**, *39*, 3798.
(31) Schlüter, D.; Müller-Buschbaum, H. Eine perowskitstaplevariante mit geordneter metallverteilung: $Ba_6Al_2Rh_2Ho_2O_{15}$. *J. Alloys Compd.* **1993**, *191*, 305−308.
(32) Kresse, G.; Furthmüller, J. Efficient Iterative Schemes for *ab initio* Total-energy Calculations Using a Plane-wave Basis Set. *Phys. Rev. B: Condens. Matter Mater. Phys.* **1996**, *54*, 11169−11186.
(33) Kresse, G.; Furthmüller, J. Efficiency of ab-initio Total Energy Calculations for Metals and Semiconductors Using a Plane-wave Basis Set. *Comput. Mater. Sci.* **1996**, *6*, 15−50.
(34) Blöchl, P. E. Projector Augmented-wave Method. *Phys. Rev. B: Condens. Matter Mater. Phys.* **1994**, *50*, 17953−17979.
(35) Kresse, G.; Joubert, D. From Ultrasoft Pseudopotentials to the Projector Augmented-wave Method. *Phys. Rev. B: Condens. Matter Mater. Phys.* **1999**, *59*, 1758−1775.
(36) Perdew, J. P.; Burke, K.; Ernzerhof, M. Generalized Gradient Approximation Made Simple. *Phys. Rev. Lett.* **1996**, *77*, 3865−3868.
(37) Saal, J. E.; Kirklin, S.; Aykol, M.; Meredig, B.; Wolverton, C. Materials design and discovery with high-throughput density functional theory: The Open Quantum Materials Database (OQMD). *JOM* **2013**, *65*, 1501−1509.

https://dx.doi.org/10.1021/acs.inorgchem.0c00936
Inorg. Chem. 2020, 59, 9699−9709

(38) Kirklin, S.; Saal, J. E.; Meredig, B.; Thompson, A.; Doak, J. W.; Aykol, M.; Rühl, S.; Wolverton, C. The Open Quantum Materials Database (OQMD): Assessing the Accuracy of DFT Formation Energies. *npj Comput. Mater.* **2015**, *1*, 15010.
(39) Jain, A.; Ong, S. P.; Hautier, G.; Chen, W.; Richards, W. D.; Dacek, S.; Cholia, S.; Gunter, D.; Skinner, D.; Ceder, G.; Persson, K. A. Commentary: The Materials Project: A materials genome approach to accelerating materials innovation. *APL Mater.* **2013**, *1*, 011002.
(40) Bugaris, D. E.; zur Loye, H.-C. Materials discovery by flux crystal growth: quaternary and higher order oxides. *Angew. Chem., Int. Ed.* **2012**, *51*, 3780−3811.
(41) Zhao, Q.; Nellutla, S.; Son, W. J.; Vaughn, S. A.; Ye, L.; Smith, M. D.; Caignaert, V.; Lufaso, M.; Pekarek, T. M.; Smirnov, A. I.; Whangbo, M. H.; zur Loye, H.-C. $Ba_4KFe_3O_9$: A Novel Ferrite Containing Discrete 6-Membered Rings of Corner-sharing FeO_4 Tetrahedra. *Inorg. Chem.* **2011**, *50*, 10310−10318.
(42) Kim, S.-H.; Yeon, J.; Halasyamani, P. S. Noncentrosymmetric Polar Oxide Material, Pb_3SeO_5: Synthesis, Characterization, Electronic Structure Calculations, and Structure-Property Relationships. *Chem. Mater.* **2009**, *21*, 5335−5342.
(43) Nguyen, S. D.; Yeon, J.; Kim, S.-H.; Halasyamani, P. S. $BiO(IO_3)$: A New Polar Iodate that Exhibits an Aurivillius-Type $(Bi_2O_2)^{2+}$ Layer and a Large SHG Response. *J. Am. Chem. Soc.* **2011**, *133*, 12422−12425.
(44) Yeon, J.; Kim, S.-H.; Nguyen, S. D.; Lee, H.; Halasyamani, P. S. Two New Noncentrosymmetric (NCS) Polar Oxides: Syntheses, Characterization, and Structure-Property Relationships in $BaMTe_2O_7$ ($M = Mg^{2+}$ or Zn^{2+}). *Inorg. Chem.* **2012**, *51*, 2662−2668.
(45) Richerson, D. W.; Hummel, F. A. Synthesis and Thermal Expansion of Polycrystalline Cesium Minerals. *J. Am. Ceram. Soc.* **1972**, *55*, 269.
(46) Scott, J. F. Ferroelectrics go bananas. *J. Phys.: Condens. Matter* **2008**, *20*, No. 021001/1.
(47) Yeon, J.; Sefat, A. S.; Tran, T. T.; Halasyamani, P. S.; zur Loye, H.-C. Crystal Growth, Structure, Polarization, and Magnetic Properties of Cesium Vanadate, $Cs_2V_3O_8$: a Structure-property Study. *Inorg. Chem.* **2013**, *52*, 6179−6186.
(48) Cohen, R. E. Origin of ferroelectricity in perovskite oxides. *Nature* **1992**, *358*, 136−138.
(49) Günter, P. Spontaneous Polarization and Pyroelectric Effect in $KNbO_3$. *J. Appl. Phys.* **1977**, *48* (8), 3475−3477.
(50) Stoumpos, C. C.; Frazer, L.; Clark, D. J.; Kim, Y. S.; Rhim, S. H.; Freeman, A. J.; Ketterson, J. B.; Jang, J. I.; Kanatzidis, M. G. Hybrid Germanium Iodide Perovskite Semiconductors: Active Lone Pairs, Structural Distortions, Direct and Indirect Energy Gaps, and Strong Nonlinear Optical Properties. *J. Am. Chem. Soc.* **2015**, *137*, 6804−6819.
(51) Xia, C.; Jia, Y.; Tao, M.; Zhang, Q. Tuning the Band Gap of Hematite α-Fe_2O_3 by Sulfur Doping. *Phys. Lett. A* **2013**, *377*, 1943−1947.
(52) Hassan, Q. U.; Yang, D.; Zhou, J. P.; Lei, Y. X.; Wang, J. Z.; Awan, S. U. Novel Single-Crystal Hollandite $K_{1.46}Fe_{0.8}Ti_{7.2}O_{16}$ Microrods: Synthesis, Double Absorption, and Magnetism. *Inorg. Chem.* **2018**, *57*, 15187−15197.
(53) Guo, Z.-Q.; Miao, N.-X.; Zhou, J.-P.; Lei, Y.-X.; Hassan, Q. U.; Zhou, M.-M. Novel Magnetic Semiconductor $Na_2Fe_2Ti_6O_{16}$: Synthesis, Double Absorption and Strong Adsorptive Ability. *J. Mater. Chem. A* **2017**, *5*, 17589−17600.
(54) Ferreira, T.; Morrison, G.; Chance, W. M.; Calder, S.; Smith, M. D.; zur Loye, H.-C. $BaFe_4O_7$ and $K_{0.22}Ba_{0.89}Fe_4O_7$: Canted Antiferromagnetic Diferrites with Exceptionally High Magnetic Ordering Temperatures. *Chem. Mater.* **2017**, *29*, 2689−2693.
(55) Xie, L. − S.; Jin, G.-X.; He, L.; Bauer, G. E. W.; Barker, J.; Xia, K. First-principles Study of Exchange Interactions of Yttrium Iron Garnet. *Phys. Rev. B: Condens. Matter Mater. Phys.* **2017**, *95*, 014423.
(56) Qian, B.; Lee, J.; Wang, G. C.; Kumar, P.; Fang, M. H.; Liu, T. J.; Fobes, D.; Pham, H.; Spinu, L.; Wu, X. S.; Green, M.; Lee, S. H.; Mao, Z. Q.; Hu, J. Ferromagnetism in CuFeSb: Evidence of Competing Magnetic Interactions in Iron-based Superconductors. *Phys. Rev. B: Condens. Matter Mater. Phys.* **2012**, *85*, 144427.
(57) Drokina, T. V.; Petrakovskii, G. A.; Molokeev, M. S.; Misyul, S. V.; Bondarev, V. S.; Velikanov, D. A.; Frontzek, M.; Schefer, J. Crystal and Magnetic Structures, Phase Transitions in Quasi-one-dimensional Pyroxenes $Na_{0.5}Li_{0.5}FeGe_2O_6$. *J. Magn. Magn. Mater.* **2015**, *385*, 243−249.

https://dx.doi.org/10.1021/acs.inorgchem.0c00936
Inorg. Chem. 2020, 59, 9699−9709